Journal of Orthopaedic Translation 23 (2020) 29–37

Contents lists available at ScienceDirect

Journal of Orthopaedic Translation

journal homepage: www.journals.elsevier.com/journal-of-orthopaedic-translation

Original Article

Wnt10b-overexpressing umbilical cord mesenchymal stem cells promote critical size rat calvarial defect healing by enhanced osteogenesis and VEGF-mediated angiogenesis

Yong Liu [a,☆], Jiarui Fang [a,☆], Quan Zhang [b], Xiaoguang Zhang [a], Yulin Cao [a], Wei Chen [d], Zengwu Shao [a], Shuhua Yang [a], Dongcheng Wu [b,c], Man Hung [e], Yingze Zhang [d], Wei Tong [a,**], Hongtao Tian [a,*]

[a] Department of Orthopaedics, Union Hospital, Tongji Medical College, Huazhong University of Science and Technology, 1277, Jiefang Avenue, Wuhan, Hubei, 430022, China
[b] Wuhan Hamilton Biotechnology Co., Ltd, Wuhan, Hubei, 430075, China
[c] Department of Biochemistry and Molecular Biology, School of Basic Medical Sciences, Wuhan University, China
[d] The Third Hospital of Hebei Medical University, 139, Ziqiang Road, Shi Jiazhuang, Hebei, 050051, China
[e] College of Dental Medicine, Roseman University of Health Sciences, 10984 S River Front Pkwy, South Jordan, UT, 84095, USA

ARTICLE INFO

Keywords:
Angiogenesis
Bone regeneration
Umbilical cord MSCs
Wnt signalling pathway

ABSTRACT

Background/objectives: Accelerating the process of bone regeneration is of great interest for surgeons and basic scientists alike. Recently, umbilical cord mesenchymal stem cells (UCMSCs) are considered clinically applicable for tissue regeneration due to their noninvasive harvesting and better viability. Nonetheless, the bone regenerative ability of human UCMSCs (HUCMSCs) is largely unknown. This study aimed to investigate whether Wnt10b-overexpressing HUCMSCs have enhanced bone regeneration ability in a rat model.

Method: A rat calvarial defect was performed on 8-week old male Sprague Dawley rats. Commercially purchased HUCMSCs^{Emp} in hydrogel, HUCMSCs^{Wnt10b} in hydrogel and HUCMSCs^{Wnt10b} with IWR-1 were placed in the calvarial bone defect right after surgery on rats ($N = 8$ rats for each group). Calvaria were harvested for micro-CT analysis and histology four weeks after surgery. CFU-F and multi-differentiation assay by oil red staining, alizarin red staining and RT-PCR (real-time polymerase chain reaction) were performed on HUCMSCs^{Emp} and HUCMSCs^{Wnt10b} *in vitro*. Conditioned media from HUCMSCs^{Emp} and HUCMSCs^{Wnt10b} were collected and used to treat human umbilical cord vein endothelial cells in Matrigel to access vessel formation capacity by tube formation assay.

Results: Alizarin red staining, oil red staining and RT-PCR results showed robust osteogenic differentiation but poor adipogenic differentiation ability of HUCMSCs^{Wnt10b}. Furthermore, HUCMSCs^{Wnt10b} could accelerate bone defect healing, which was likely due to enhanced angiogenesis after the HUCMSCs^{Wnt10b} treatment, because more CD31+ vessels and increased vascular endothelial growth factor-A (VEGF-A) expression were observed, compared with the HUCMSCs^{Emp} treatment. Conditioned media from HUCMSCs^{Wnt10b} also induced endothelial cells to form vessel tubes in a tube formation assay, which could be abolished by SU5416, an angiogenesis inhibitor.

Conclusion: To our knowledge, this is the first study providing empirical evidence that HUCMSCs^{Wnt10b} can enhance their ability to heal calvarial bone defects via VEGF-mediated angiogenesis.

The translational potential of this article: HUCMSCs^{Wnt10b} can accelerate critical size calvaria and are a new promising therapeutic cell source for fracture nonunion healing.

* Corresponding author. Department of Orthopaedics, Union Hospital, Tongji Medical College, Huazhong University of Science and Technology, 1277, Jiefang Avenue, Wuhan, Hubei, 430022, China.
** Corresponding author. Department of Orthopaedics, Union Hospital, Tongji Medical College, Huazhong University of Science and Technology, 1277, Jiefang Avenue, Wuhan, Hubei, 430022, China.
E-mail addresses: 961836059@qq.com (Y. Liu), fangjiarui1992@163.com (J. Fang), 470558642@qq.com (Q. Zhang), zhangxiaoguang0095@163.com (X. Zhang), caoyulin1220@126.com (Y. Cao), 754958715@qq.com (W. Chen), 381712554@qq.com (Z. Shao), 1010948762@qq.com (S. Yang), bcdcwu@hotmail.com (D. Wu), mhung@roseman.edu (M. Hung), 258974810@qq.com (Y. Zhang), tongwei312@126.com (W. Tong), tianhongtao@vip.163.com (H. Tian).
☆ Yong Liu and Jiarui Fang contributed equally.

https://doi.org/10.1016/j.jot.2020.02.009
Received 23 October 2019; Received in revised form 8 February 2020; Accepted 13 February 2020
Available online 28 March 2020

Introduction

Of more than 6.2 million fractures that occur each year, fracture healing is not perfect and still fails occasionally, resulting in 5–10% of delayed or nonunion healing [1]. These failures are a substantial physical, medical and financial burden for affected individuals and our society. Therefore, developing a strategy for promoting bone regeneration is a crucial issue for both surgeons and basic scientists.

Cell therapy is a promising strategy to promote the healing process. Tissue-specific mesenchymal stem cells share self-renewal and multi-differentiation capacity, so they are a good source of cells for transplantation to regenerate tissue [2]. These cells can be derived from different tissues, such as bone marrow, adipose tissue, umbilical cord tissue and so on. Among the different types of therapeutic cells, bone marrow mesenchymal stem cells (BMSCs) have been considered the gold standard from early research to the modern cell-based therapies. Other tissue-specific stem cells, such as adipose-derived stem cells, also showed promising bone healing effects. However, the painful and invasive collection method for cells has become a substantial drawback for large-scale clinical applications. Additionally, isolated cells are generally from adult tissue with relatively diminished self-renewal and differentiation capacity compared with stem cells from foetal tissue [3]. Therefore, a more feasible source of stem cells is needed.

Human umbilical cord mesenchymal stem cells (HUCMSCs) coming from the umbilical cord are reported to be highly proliferative [4]. Unlike BMSCs [5], they represent a noncontroversial source of tissue-specific stem cells that are noninvasively collected. Therefore, HUCMSCs are probably more suitable for clinical application, such as heart disease [6], Alzheimer's disease [7] and osteoarthritis [8]. Exosomes from HUCMSCs for rat long bone fracture healing [9] possibly *via* Wnt signalling pathway [10] or HUCMSCs alone could promote rat calvarial defect healing. However, in an *in vitro* study, HUCMSCs showed relatively weak osteogenic differentiation ability compared to BMSCs [11]. A clinical study demonstrated that HUCMSCs combined with BMPs could effectively promote femoral shaft fracture healing [12]. Thus, it is of great interest to improve the osteogenic differentiation ability of HUCMSCs to obtain robust bone healing effects.

Wnt signalling pathway plays an essential role in bone development and regeneration. Among 19 Wnt ligands, the inhibition of Wnt10b from pre-adipocytes can result in an approximately 50% decrease in fat tissue [13], with a FABP-Wnt10b mouse model exhibiting a three-fold increase in bone due to Wnt10b upregulation [14]. Furthermore, Wnt10b expression can maintain the stemness of stem cells and promote bone regeneration [15]. Dysregulation of Wnt10b can lead to impaired vasculature formation in the yolk sac [16]. Therefore, Wnt10b has the potential to promote bone defect healing by enhancing both osteogenesis and angiogenesis.

In this study, we generated HUCMSCs^{Wnt10b}, which were transduced with a lentivirus that enabled overexpression of the Wnt10b ligand, and we hypothesised that these cells possess an improved bone regeneration ability. Even though HUCMSCs^{Wnt10b} possess a robust CFU-F and osteogenic differentiation ability, they have a limited adipogenic differentiation capacity *in vitro*. In a critical size rat calvarial defect model, treatment with HUCMSCs^{Wnt10b} can significantly accelerate the bone healing process and induce increased vascular endothelial growth factor-A (VEGF-A) expression and formation of CD31+ blood vessels; yet these effects may be greatly diminished by treatment with IWR-1, which is a commonly used Wnt signalling pathway inhibitor. A tube formation assay was performed and showed that human umbilical vein endothelial cells (HUVECs) cultured in conditioned media from HUCMSCs^{Wnt10b} exhibited more angiogenesis than HUVECs cultured in empty vector-transduced HUCMSCs (HUCMSCs^{Emp}) conditioned media that is abolished by the angiogenesis inhibitor SU5416. These findings suggest that HUCMSCs^{Wnt10b} can promote bone regeneration partially through enhanced osteogenesis and VEGF-mediated angiogenesis.

Methods and materials

Generation of the Wnt10b-lentivirus expression vector

The Sprague Dawley (SD) rat kidney RNA, reverse transcription synthesised cDNA containing the Wnt10b gene was used as a template for amplification of the Wnt10b gene by nested PCR (polymerase chain reaction). The products were digested with the restriction endonucleases NheI and XhoI and then inserted into the lentivirus vector pHAGE-CMV-MCS-IRES-Zsgreen to construct a CMV single promoter vector named pHAGE-CMV-MCS-IRES-Zsgreen-Wnt10b. After transformation into competent *E. coli* cells, positive clones as verified by colony PCR were sent to Tian Yi Hui Yuan at Biotechnology Co., Ltd. for sequencing verification.

Lentivirus package

When 293T cells (Shanghai Pito, PT-00453) were in the logarithmic growth phase, 4×10^6 cells were seeded in 6-well plates. When cells covered 90% of every well, the culture medium of DMEM (Gibco, 8118409) with 10% FBS was removed, and pHAGE-CMV-MCS-IRES-Zsgreen-Wnt10b, pSPAX2 and pMD2G were added to transfect the 293T cells. Green fluorescence was observed under a fluorescence microscope, and 72 h after transfection the supernatant was collected and ultracentrifuged (4°C, 70,000 g, 2 h) to concentrate the lentivirus. The lentivirus concentrate was then stored at −80°C.

Preparation of Wnt10b-overexpressing HUCMSCs

HUCMSCs were purchased from Wuhan Hamilton Biotechnology Co., Ltd. HUCMSCs (4×10^6) were seeded in a 6-well plate, and when cells covered 90% of every well, the medium (Cyagen, HUXUC-03061) was changed, and the lentivirus was added. The lentivirus was packaged previously, and it was added to generate HUCMSCs^{Wnt10b}. Empty vector-transduced HUCMSCs (HUCMSCs^{Emp}) were used as controls in the study. Cells were cultured with growth media (Cyagen, HUXUC-03061), and P5–P7 were used for experiments.

Real-time polymerase chain reaction

To investigate whether HUCMSCs^{Wnt10b} could overexpress WNT10B gene, total RNA was isolated using TRIzol (Invitrogen). The total RNA (200–500 ng) was extracted for reverse transcription synthesis using the High-Capacity cDNA Reverse Transcription Kit (Applied Biosystems). The relative level of expression of each target gene was analysed using the $2^{-\Delta\Delta CT}$ method after real-time polymerase chain reactions (RT-PCRs). The primer sequences used in this study are listed in Table S1.

Western blot

In order to examine whether HUCMSCs^{Wnt10b} could activate overexpression of Wnt10b protein and Wnt signalling pathway, total protein was extracted and its concentration was determined by the BCA assay. Next, proteins were subjected to electrophoresis under reducing conditions and blotted onto a polyvinylidene difluoride membrane. Membranes were then incubated with primary antibody (1:100): anti-Wnt10b antibody (ab66721, abcam), anti-β-catenin antibody (610153, B&D) and GAPDH (60004-1-1g, proteintech). Secondary antibody in TBST was diluted with 5% milk and incubated with membranes for 40–60 min at room temperature with agitation. Signals were detected with ECL using an electrochemiluminescence kit.

Conditioned media collecting

HUCMSCs^{Emp} and HUCMSCs^{Wnt10b} were cultured in the growth media until they were of 80–90% confluence and then washed with PBS for three times. Then a-MEM (Gibco, 12571063) was treated for 12 h.

Conditioned media were collected and centrifuged to get rid of cell debris. Upper media were collected, aliquoted and stored in −20°C.

Differentiation assay

To determine whether Wnt10b protein could promote the osteogenic and adipogenic differentiation ability of MSCs, a series of cell differentiation assays were performed. For adipogenic differentiation assay, HUCMSCs and HUCMSCs^{Wnt10b} were seeded at 2×10^5/well in a 6-well plate with growth media, adipogenic media (Cyagen, HUXUC-90031). At 80–90% confluence, cells were incubated with different media: growth media, osteogenic media and osteogenic media with Wnt pathway inhibitor, IWR-1 (MCE, Cat. No: HY-12238). After 14 days, oil red staining was performed. For osteogenic differentiation assay, HUCMSCs and HUCMSCs^{Wnt10b} were seeded at 2×10^5/well in a 6-well plate with growth media and osteogenic media (Cyagen, HUXUC-90021). When they reached 80–90% confluence the next day, cells were incubated with a different set of media: growth media, osteogenic media and osteogenic media with Wnt pathway inhibitor IWR-1. Alizarin red staining was also performed. After staining, the area of oil red staining or alizarin red staining was measured by ImageJ, and the staining area per total area was reported. The adipogenic gene (i.e., PPAR-γ, CEBP and LPL) and the osteogenic gene (i.e., OCN, OSX and IBSP) were measured by RT-PCR. To determine if the Wnt signalling was active, the β-catenin gene was measured by RT-PCR and the β-catenin protein was measured by Western blot.

CFU-F assay

HUCMSCs^{Emp} and HUCMSCs^{Wnt10b} were seeded at 5000 cells/well of a 6-well plate in growth media. After 7 days, cells were washed with PBS for three times and then fixed in 4% paraformaldehyde for 20 min. The cells were then stained using 1% crystal violet for 10 min and the wells were washed with PBS for three times. The number of colonies was calculated.

Tube formation assay

The human umbilical vein endothelium cells (HUVECs, ATCC, ATCCCRL-1730) were cultured in a T-25 culture flask with an endothelial cell culture medium (ScienCell, 1001). Matrigel (50 μl) (BD, 356234) was added into the well of a 96-well plate and kept in 37°C for 1 h. HUVECs (20,000) were seeded in each well in different conditioned media: (1) conditioned media from HUCMSCs^{Emp} and (2) conditioned media from HUCMSCs^{Wnt10b}, with or without SU5416 (Sigma, S8442). After 4 h, the HUVECs were observed using a light microscope and the number of branch points and tube numbers were calculated.

Rat calvarial bone defect model

The critical size calvarial defect model was prepared as previously described [17]. Briefly, male SD rats at 8 weeks of age were used. A 1–1.5 cm incision was made to the periosteum. The calvarium was drilled with the surgical drill (5 mm diameter) until the dura mater was exposed. The diameter of the hole in the rat calvarium was measured to ensure that the hole was 5 mm in diameter. The defect was copiously washed with sterile normal saline to remove any debris and bone chips. Different treatments were as follows:

Group 1: rat defects were treated with vehicle (saline); Group 2: rat defects were seeded with hydrogel only; Group 3: rat defects were seeded with HUCMSCs^{Emp} in hydrogel; Group 4: rat defects were seeded with HUCMSCs^{Wnt10b} in hydrogel; and Group 5: rat defects were seeded with HUCMSCs^{Wnt10b} in hydrogel and treated with IWR-1 (10 μM/L). Each of the five groups had a sample size of eight. Hydrogel was used to support cells locally and prevent leakage; cells (1×10^5) were mixed with an equal volume of commercially purchased hydrogel (BD™, Catalogue No. 354250) and placed into the defect.

Micro-CT analysis

The rat calvaria were harvested 28 days after the operation and fixed with 4% paraformaldehyde for 48 h. Then, they were scanned with a SkyScan 1176 high-resolution micro-CT imaging system (Bruker, USA) at an 18 μm resolution with a 1 mm aluminium filter, a voltage of 90 kV and a current of 273 μA. Volumetric reconstruction and analysis were conducted using NRecon and CT-analyser software provided by SkyScan. A scoring guide was used to assess the extent of bony bridging and union defects using micro-CT datasets [18,19].

Histology

Samples after micro-CT analysis were decalcified and processed for histology. After decalcifying the skull in 15% EDTA for 30 days, all samples were dehydrated in a graded series of ethanol (from 70% to 100%) and embedded in paraffin. Then, 6-μm-thick sections of the defect area were cut sagittally and submitted to HE and Masson staining. Three sections from each sample (1/4, 1/2 and 3/4 from the edge of the defect area) were selected for scoring [17].

Paraffin sections were also used for immunohistochemistry after appropriate antigen retrieval, and slides were incubated at 4°C overnight with primary antibodies as follows: anti-CD31 (1:100, BD, 555025), anti-VEGFA (1:100, Abcam, ab46154) and anti-Col-1 (1:100, Boster, Ba0325). That incubation was followed by binding with biotinylated secondary antibodies and then DAB (DakoCytomation, #K3465) for colour development.

Statistical analyses

Results from descriptive statistics were expressed as mean ± standard error of the mean (SEM). All statistical analyses were conducted using GraphPad Prism. Comparisons between groups were analysed by either a Student *t* test (paired or unpaired as appropriate) or one-way or two-way ANOVA (with repeated measurements as appropriate) with Bonferroni's post-hoc test to adjust for multiplicity. A p value of less than 0.05 was considered statistically significant.

Results

HUCMSCs^{Wnt10b} exhibit robust Wnt10b expression

Using the lentivirus gene transduction method, we incorporated the WNT10B gene, a well-known bone regeneration promoting regulator, into HUMSCs. After transduction, the new cells, HUCMSCs^{Wnt10b}, showed enriched expression of stem cell markers CD105 (99.7%), CD73 (100%) and CD90 (99.7%) and low expression of hematopoietic lineage cell markers CD45 (0%) and CD14 (0.2%) (Fig. 1A), demonstrating that HUCMSCs^{Wnt10b} still expressed high levels of stem cell markers after transduction. Aligning with expectation, the results from RT-PCR showed an up to 20-fold increase in WNT10B levels in HUCMSCs^{Wnt10b} comparing to the levels found in the HUCMSCs^{Emp} (Fig. 1B). To confirm the change at the protein level, we harvested total protein and performed Western blot analyses, which revealed a dramatic increase in Wnt10b protein expression in HUCMSCs^{Wnt10b} compared to the control (Fig. 1C). In addition, β-catenin PCR and Western blot analyses confirmed the increase in Wnt β-catenin signalling pathway (Fig. 1D and E). These results clearly showed that Wnt10b-overexpressing HUCMSCs, HUCMSCs^{Wnt10b}, had been successfully generated.

Characterisation of HUCMSCs^{Wnt10b} stemness

To characterise the viability of transduced cells, we performed cell culture experiments. First, we cultured both the transduced and control cells in growth media at a low density. HUCMSCs^{Wnt10b} generated 33 colonies per 5000 cells, which represented 1.4-fold increase in CFU-F

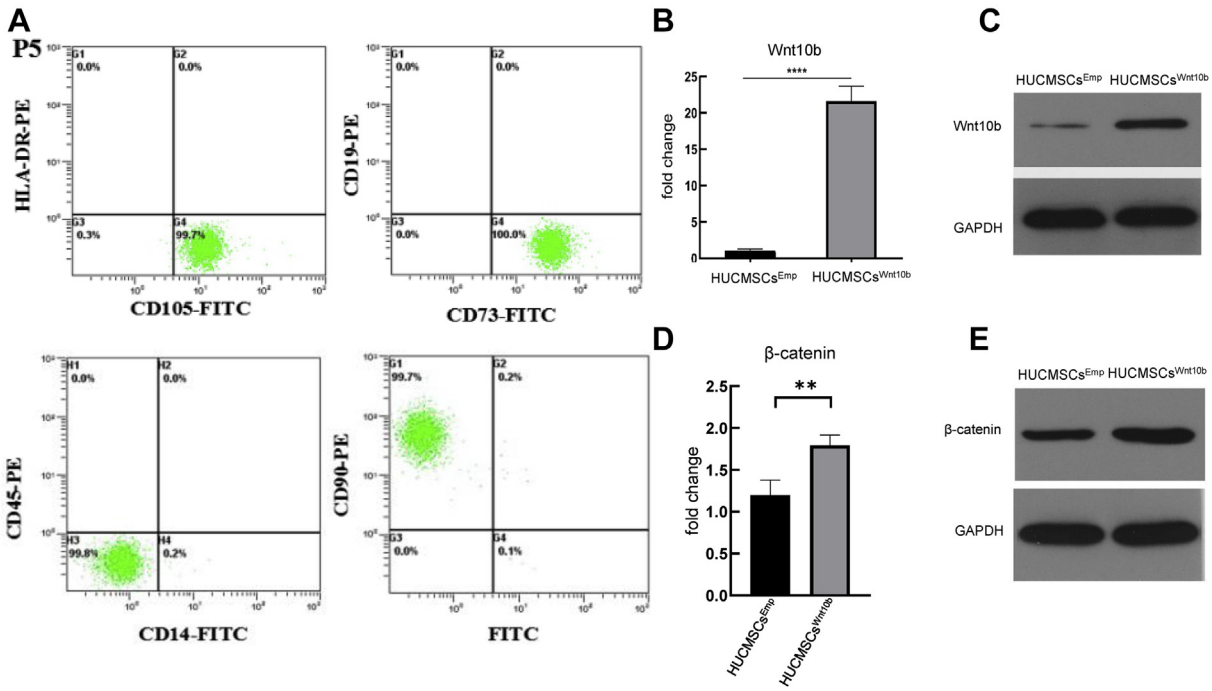

Figure 1. HUCMSCs^{Wnt10b} exhibited a mesenchymal stem cell phenotype and overexpressed the Wnt10b gene and protein. (A) Flow cytometry analysis revealed that HUCMSCs^{Wnt10b} exhibit a stem cell marker phenotype. (B) The expression of the WNT10B gene was assessed by RT-PCR. (C) The expression of Wnt10b protein was assessed by Western blot in HUCMSCs^{Wnt10b} and HUCMSCs^{Emp}, (B) and (C) show that the relative expression of Wnt-10b in HUCMSCs^{Wnt10b} was significantly higher than it was in HUCMSCs^{Emp} (mean ± SEM, ****: $p < 0.0001$, Student *t* test is used for statistics). (D) The expression of the β-catenin gene was assessed by RT-PCR. (E) The expression of β-catenin protein was assessed by Western blot in HUCMSCs^{Wnt10b} and HUCMSCs^{Emp}, (D) and (E) show that the Wnt signalling was activated (mean ± SEM, **: $p < 0.01$, Student *t* test is used for statistics). The results are representative of at least three independent experiments. HUCMSCs^{Emp}: empty vector transduced HUCMSCs.

colonies compared to the control that had 24 colonies (Fig. 2A and B). These results indicated that HUCMSCs^{Wnt10b} had robust self-renewal ability compared with the control. To explore the multi-differentiation ability of HUCMSCs^{Wnt10b}, we cultured the cells in adipogenic differentiation media but found less oil red staining in the HUCMSCs^{Wnt10b} group compared with the control (Fig. 2C and E). In addition, RNA was harvested for RT-PCR, and in HUCMSCs^{Wnt10b}, we found a significant decrease in PPAR-γ, CEBP and LPL, which are genes that are typically expressed during adipogenic differentiation (Fig. 2F). Furthermore, this inhibited effect, both demonstrated by oil red staining and RT-PCR results, could be reversed by treating HUCMSCs^{Wnt10b} with IWR-1, a Wnt signalling pathway inhibitor (Fig. 2C, E and F). To compare the osteogenic differentiation ability, we cultured those cells in osteogenic differentiation media and found that HUCMSCs^{Wnt10b} exhibited enhanced alizarin red staining and expression of osteoblastic genes, such as OCN, OSX and IBSP; these results demonstrated that HUCMSCs^{Wnt10b} had robust osteogenic differentiation capability, yet the effect could be diminished by IWR-1 (Fig. 2D, E and G). These effects were positively correlated with β-catenin expression (Supplementary Figure 1). In summary, HUCMSCs^{Wnt10b} exhibited a high self-renewal capacity, osteogenic differentiation ability and inhibited adipogenic differentiation, which was likely due to the effect resulting from Wnt10b secretion by HUCMSCs^{Wnt10b}.

HUCMSCs^{Wnt10b} promoted bone defect repair in a critical size rat calvarial defect model

After we observed enhanced osteogenic differentiation ability *in vitro*, we performed *in vivo* studies to further explore the bone regeneration ability in a critical size rat calvarial defect model. We seeded 1×10^5 HUCMSCs^{Emp} and HUCMSCs^{Wnt10b} into a commercially purchased hydrogel in order to provide a stable local environment for the cells; we placed the mix into a skull defect with a diameter of 5 mm. Subsequent 3D reconstructed micro-CT images showed that veh- and gel-treated defects showed an obvious defect at the 4-week time point, with slight bone formation occurring along the border of the defect; HUCMSCs treatment had moderate healing from the edge of the defect area with an obvious defect in the centre. Surprisingly, HUCMSCs^{Wnt10b} could heal the defect area with virtually no empty space in the defect area, the effects of which were greatly abolished by HUCMSCs^{Wnt10b} + IWR-1 combined treatment (Fig. 3A). In line with this observation, micro-CT-based analysis showed that both the veh- and gel-treated groups had similar defect volumes at the 4-week time point: 3.06 ± 0.17 and 3.84 ± 0.19 mm^3, respectively. However, the HUCMSCs^{Emp} treatment decreased the volume to 2.45 ± 0.09 mm^3. The HUCMSCs^{Wnt10b} treatment further decreased the volume to 1.63 ± 0.16 mm^3, which was 67% of the size that remained after the HUCMSCs^{Emp} treatment. Yet this healing effect of HUCMSCs^{Wnt10b} was dramatically blocked by IWR-1; the defect volume in that group was 3.6 ± 0.12 mm^3, which resembled the results in the veh- and gel-treated groups (Fig. 3B). Furthermore, using a scoring system to assess the bony bridging across the defect [19], similar observation was found. An average score of 3.8 ± 0.17 was found in the HUCMSC^{Wnt10b}-treated defect, which was significantly better than the HUCMSCs^{Emp}-treated group score (2.8 ± 0.37), the veh-treated group score (2.3 ± 0.33) and the gel-treated group score (2.3 ± 0.25). Interestingly, a combined treatment of IWR-1 in HUCMSCs^{Wnt10b} decreased the score from 3.8 ± 0.17 to 2.3 ± 0.33, which demonstrated a Wnt signalling pathway-dependent healing by HUCMSCs^{Wnt10b} (Fig. 3C). In summary, slight healing from the edge could be found in the veh- and gel-treated groups, and HUCMSCs^{Emp} had moderate bone healing at the 4-week time point. HUCMSCs^{Wnt10b} could significantly enhance the regenerative effects compared with HUCMSCs^{Emp}. However, this enhanced effect of HUCMSCs^{Wnt10b} was dramatically diminished by the Wnt signalling pathway inhibitor IWR-1.

Next, when we performed histological analysis on paraffin sections to more closely examine the healing tissue and to assess the defect by

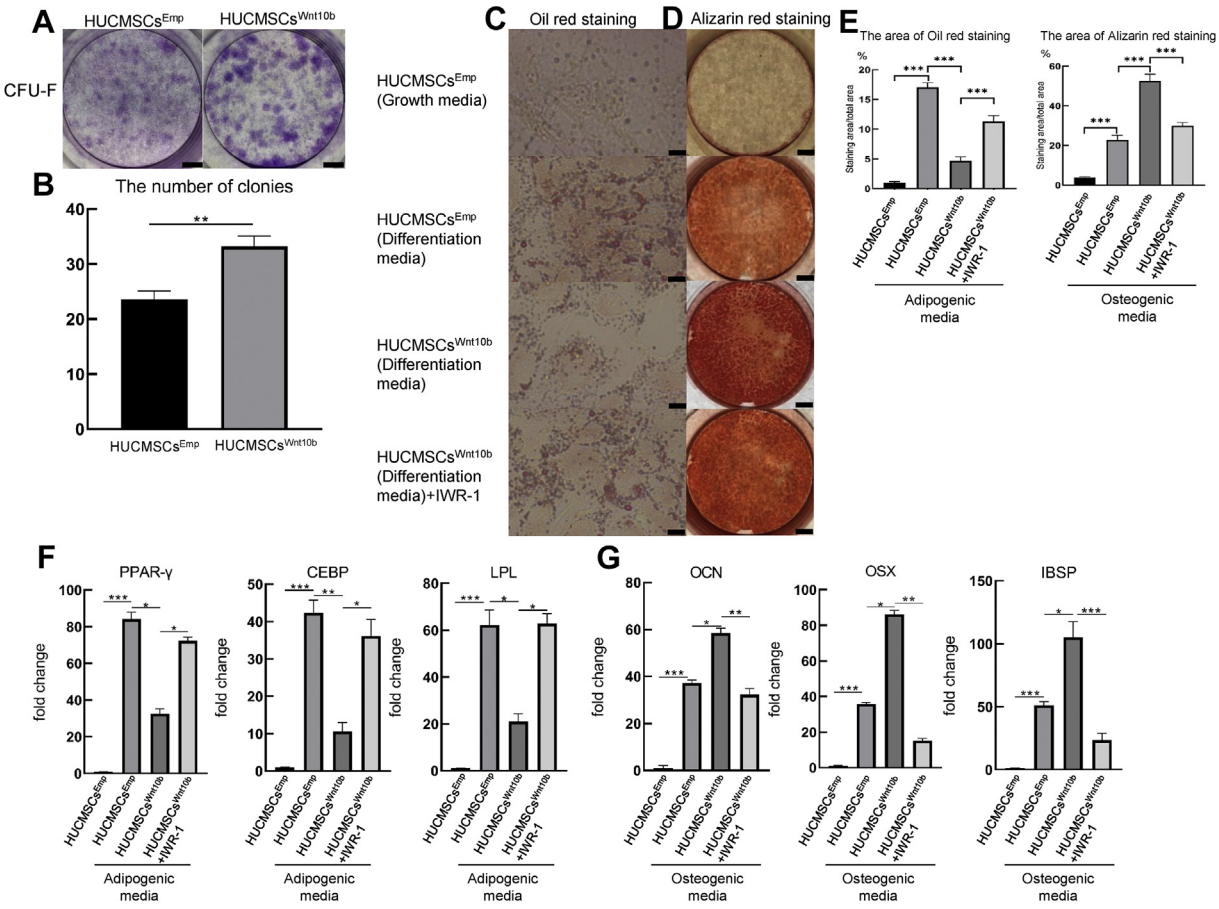

Figure 2. HUCMSCs^{Wnt10b} had robust self-renewal ability and osteogenic differentiation ability but decreased adipogenic differentiation ability. (A) The self-renewal ability of HUCMSCs^{Emp} and HUCMSCs^{Wnt10b} was assessed by CFU-F assays. HUCMSCs^{Emp} and HUCMSCs^{Wnt10b} were seeded in 6-well plates at 1000 cells/well. Seven days later, the cells were stained with crystal violet (scale bar = 0.5 mm). (B) Colonies, which contain more than 50 cells, were quantified ($n = 3$, mean ± SEM, **: $p < 0.01$, Student t test, results are representative of at least three independent experiments). (C) HUCMSCs^{Emp} cultured in growth media did not show any oil red staining after 14 days. As expected, adipogenic media caused HUCMSCs^{Emp} to have positive oil red staining; adipogenic media caused less oil red staining in HUCMSCs^{Wnt10b} until treatment with IWR-1, a Wnt signalling pathway inhibitor (scale bar = 200um). (D) HUCMSCs^{Emp} show few alizarin red staining in growth media and moderate alizarin red staining in osteogenic media, whereas HUCMSC^{Wnt10b} in osteogenic media show robust alizarin red staining, which was attenuated by IWR-1 (scale bar = 0.5 mm). (E) The areas of oil red staining and alizarin red staining were measured by ImageJ and counted ($n = 3$, mean ± SEM, ***: $p < 0.001$, Student t test, results are representative of at least three independent experiments). (F) RNA was isolated for quantitative PCR analysis of expression of adipogenic genes 14-day post confluence: PPAR-γ, CEBP and LPL. (G) The following osteogenic genes were quantified by quantitative PCR: OCN, Osx and IBSP ($n = 3$, mean ± SEM, *: $p < 0.05$, **: $p < 0.01$, ***: $p < 0.001$, Student t test, results are representative of at least three independent experiments).

measuring the defect area and perform histological scoring [19], we found several layers of fibrous tissue occupying the defect area in the veh- and gel-treated groups (see HE staining in Fig. 4A). The histology scores for the veh- and the gel-treated groups were 1.6 ± 0.54 and 1.8 ± 0.44, respectively, demonstrating very mild healing (Fig. 4B). In the HUCMSCs^{Emp}-treated group, we observed several bony islands in the fibrous tissue of the defect area, with a significantly higher score of 2.6 ± 0.54 (Fig. 4B) and a narrower defect (Fig. 4C). Furthermore, the HUCMSCs^{Wnt10b} treatment bridged the defect area with thin newly formed bone, with fibrous tissue superficially covering the bone tissue. A significantly higher histology score was observed for the HUCMSCs^{Wnt10b}-treated group, 3.75 ± 0.5 (Fig. 4A–C). The introduction of IWR-1 to the HUCMSC^{Wnt10b}-treated group clearly decreased bony bridging with fibrous tissue in the defect area, demonstrating effects similar to the veh- and gel-treated groups (Fig. 4A–C). These histology results demonstrated that the calvarial defect was filled with fibrous tissue from the vehicle and hydrogel treatments, and HUCMSCs^{Wnt10b} replaced the fibrous tissue in the defect area with bone tissue because they exhibited more robust bone regenerative effects than what was observed with HUCMSCs^{Emp}. The regenerative effects could be greatly diminished by inhibiting the Wnt signalling pathway.

As collagen-1 deposition and mineralisation play a critical role in bone formation, we performed Masson's trichrome staining, which can detect collagen fibres and bone mineralisation and thus characterise the structure of the healing tissue. At 4 weeks post-surgery, we observed strong and dense blue staining in the defect area after HUCMSCs^{Wnt10b} treatment, demonstrating collagen and mineralised bone formation. Several layers of collagen fibres (fibrous tissue) could be observed in the nonbridging area following veh, gel and HUCMSCs^{Emp} treatments as well. Once again, this robust bone-forming effect of HUCMSCs^{Wnt10b} could be diminished by IWR-1 (Fig. 4D).

HUMSCs^{Wnt10b} promote VEGF-mediated angiogenesis

Osteogenesis and angiogenesis are closely coupled during bone regeneration. In addition to more bone being formed in the HUCMSC^{Wnt10b}-treated group, we found robust Collagen-1 staining in HUCMSCs^{Wnt10b} (Fig. 5A), demonstrating a very active bone forming process. At 4-week post-surgery, we observed slightly more VEGF-A, which is an angiogenic factor, in the HUCMSCs^{Emp}-treated group compared to the hydrogel-treated group. The HUCMSCs^{Wnt10b} could obviously induce stronger VEGF-A staining locally compared with

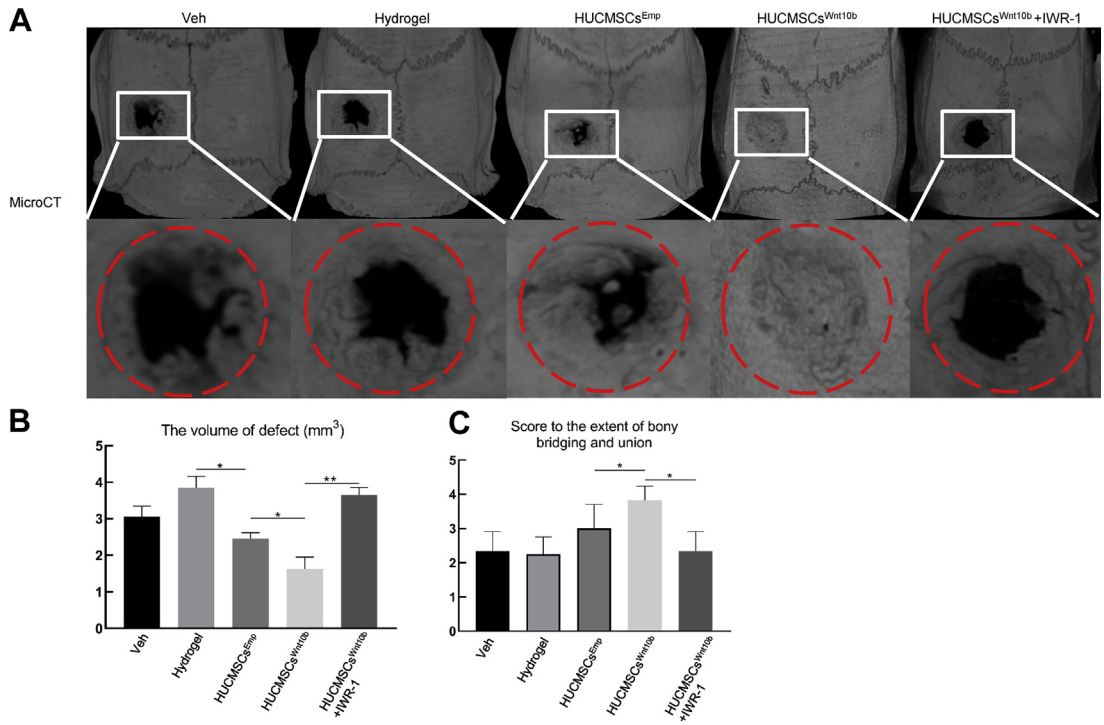

Figure 3. Micro-CT analysis demonstrated that HUCMSCs^{Wnt10b} promoted critical size defect healing in rats at 4-weeks after surgery. (A) The bone defect was treated by veh, hydrogel, HUCMSCs^{Emp}, HUCMSCs^{Wnt10b} and HUCMSCs^{Wnt10b} + IWR-1, and then each calvarium was harvested 28 days after surgery; the defect area was assessed by micro-CT analysis. (B) Average volume of defect area is shown. (C) Bony bridging and union of the defect was scored based on micro-CT images ($n = 8$, mean ± SEM, *: $p < 0.05$, **: $p < 0.01$, Student t test, results are representative of at least three independent experiments).

HUCMSCs^{Emp}, especially in the fibrous tissue superficial to the bone (Fig. 5B). As VEGF is key to blood vessel growth, we performed CD31 staining to label blood vessels. In line with the VEGF-A results, vessels were hardly seen in the fibrous tissue of the defect in the hydrogel-treated group. We observed obvious CD31+ vessels in the HUCMSCs^{Emp}-treated group and even more vessels in the HUCMSCs^{Wnt10b}-treated group (Fig. 5C). In addition, the increased VEGF-A and CD31 staining in HUCMSCs^{Wnt10b}-treated calvaria was evidently abolished by IWR-1 (Fig. 5B and C). To confirm the angiogenic effects of HUCMSCs^{Wnt10b} on endothelial cells, we performed a tube formation assay on HUVECs by culturing them in different conditioned media. Interestingly, cells grown in conditioned media from HUCMSCs^{Wnt10b} had significantly more branch points (84.4 ± 5.128 for the HUCMSCs^{Wnt10b} conditioned media and 32.4 ± 3.507 for the HUCMSCs^{Emp} conditioned media) (Fig. 5D and F) and tube numbers compared to HUCMSCs^{Emp} (Fig. 5D and E). These effects could be abolished by the introduction of SU5416 (Fig. 5D–F). Taken into consideration of both the *in vivo* and *in vitro* results, we concluded that HUCMSC^{Wnt10b} treatment could ameliorate angiogenesis, possibly through VEGF.

Discussion

Naive MSCs transplantation is sometimes not sufficient for regeneration, but could be pretreated with hypoxia to increase its viability [20,21] or co-transplanted with proangiogenic cells [22] in order to improve the regeneration effects. In addition, numerous studies investigated cell therapies with gene therapies, in which cells were modified to overexpress bone formation regulating genes to accelerate bone regeneration. For example, overexpression of PDGF-BB in HSCs increased the trabecular bone formation and decreased cortical porosity [23]. A recent study generated BMP-2-overexpressing umbilical cord blood MSCs and found effective bone repair effects [24]. As for HUCMSCs, CD61-overexpressing HUCMSCs would help promote HUCMSCs differentiation into PGC and male germ-like cells [25], and IL-10 overexpressing HUCMSCs could enhance human macrophage function, demonstrating HUMCMSCs' therapeutic potential for infection-induced acute respiratory distress syndrome (ARDS) [26]. However, to our knowledge, no transgenic HUCMSCs have been generated for bone repair.

In this study, we found HUCMSC^{Wnt10b} was prone to undergo osteogenesis and nearly 80% healing was observed in the HUCMSC^{Wnt10b}-treated group compared with 56% in the HUCMSCs^{Emp} implantation group at 4-week post-surgery. As to the sharp decrease of transplanted cells at day 14 and then the absence of the cells on day 28 [27], it is possible that the secreted Wnt10b from HUCMSCs^{Wnt10b} made a substantial contribution to the healing process through acting on endogenous stem cells, such as Prx-1+ periosteal stem cells, in the calvarium [28]. However, the exact amount of regenerated tissue that is directly contributed from the transplanted cells remains to be a question and needs to be studied in the future.

Other than the action to deliver cells and regulatory factors, we believe that transduced Wnt10b also alters HUCMSCs viability via an autocrine mechanism, which helps defect healing. In this study, we found gene expression of typical osteogenic differentiation markers OCN, OSX and IBSP, elevated up to a 100-fold change, while adipogenic differentiation markers PPAR-γ, LPL and CEBP were all significantly downregulated. This is in line with a previous study showing that pluripotent mesenchymal precursors (ST2 cells) that overexpressed Wnt10b expressed a significantly high level of osteoblast transcription factors (Runx2, Osx and Dlx5), and ST2 cells could rescue bone volume in an OVX-induced osteoporosis model [14]. In addition, transcripts expressed during adipogenic differentiation (PPAR-γ, CEBPa and FABP4) were downregulated [14] and fat tissue formation was inhibited [13]. This exclusive switch between the osteogenesis differentiation capacity and the adipogenesis differentiation capacity of MSCs is critical for enhanced bone regeneration of transplanted cells. Importantly for the first time, we found an obvious increase in the number of CFU-F colonies formed by HUCMSCs^{Wnt10b}, which implicated a robust self-renewal capacity of stem cells by Wnt10b.

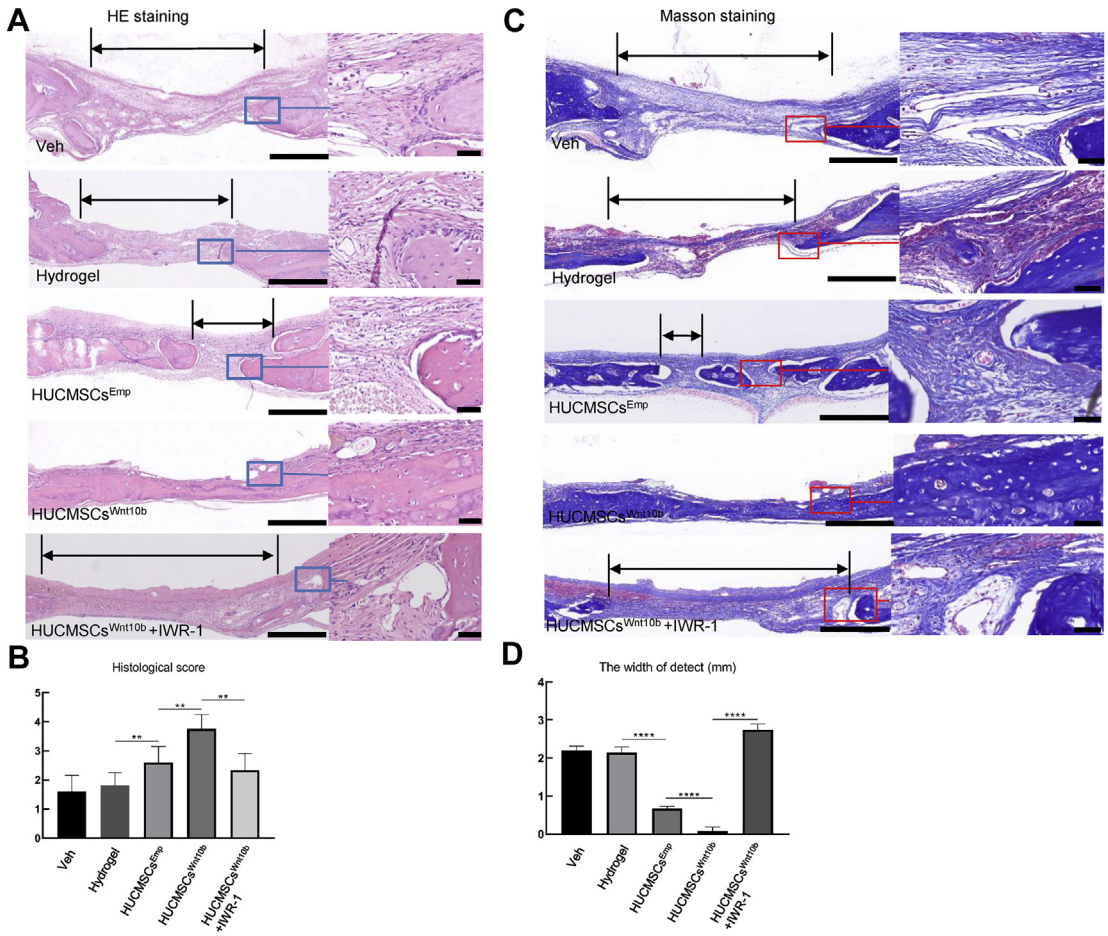

Figure 4. Histology showed enhanced mineralising bone and collagen formation by HUCMSCs^{Wnt10b}. (A) After micro-CT analysis, samples underwent tissue processing and were stained for H&E. The area of defect is indicated by double arrows. The right panel is a magnified image of the boxed area, which is the interface between the bone and defect fibrous tissue. (B, D) Based on histology, the width of the defect area and bridging score from three sections of each sample were averaged, and then eight samples from each group were quantified for statistical analysis. (C) Masson staining for collagen and mineralisation was performed to show bone matrix and mineralisation during defect healing ($n = 8$, **: $p < 0.01$, ***: $p < 0.001$, ****, $p < 0.0001$, Student t test is used for statistics, scale bar = 500 μm (left panel), scale bar = 100 μm (zoom in image on the right panel)).

In this study, we used a rat calvarial bone critical defect that cannot be healed by itself and is considered a fracture nonunion model. We observed several layers of fibrous tissue superficially covering the defect area in the untreated group, which is consistent with findings from previous studies [18,19] and is similar to results demonstrated in the long bone fracture nonunion model [29]. After treatment with HUCMSCs^{Wnt10b}, the defect was filled with roughly normal laminar bone. Wnt10b was shown to inhibit fibrous tissue formation in this nonunion model, as Wnt10b can attenuate fibrous tissue formation after cardiac injury and thus promote repair [30]. Therefore, the inhibition of fibrous tissue formation also contributes to the accelerated healing process of HUCMSCs^{Wnt10b}.

Interestingly, we found more VEGF-A expression in HUCMSC^{Wnt10b}-treated groups than that in other groups. Kai Hu et al. have shown that reduced levels of VEGF could promote MSC differentiation into fibroblasts [31]. Therefore, the replacement of fibrous tissue with bone in the HUCMSC^{Wnt10b}-treated group may be attributed to VEGF in addition to the Wnt10b protein produced by HUCMSCs^{Wnt10b}. However, the calvarial defect model does not faithfully mimic the clinical features of fracture nonunion of long bones; the repair of flat bones such as the calvarium and the clavicle involves intramembranous ossification, while fractures in a long bone undergo endochondral ossification, which involves cartilage metabolism. In particular, Wnt signalling plays an important but complex role in chondrogenesis during endochondral ossification. Canonical Wnt signalling activation can switch chondrogenesis to osteogenesis of MSCs [32]. On the contrary, chondrocyte maturation needs certain level of activation [33]. However, we did not see a significant change on chondrocyte differentiation by HUCMSCs^{Wnt10b} in our preliminary experiment. Future studies of the effects of HUCMSCs^{Wnt10b} on long bone fracture healing and the long bone fracture nonunion model are needed.

Angiogenesis and osteogenesis play a critical role in bone defect healing. Numerous cytokines, such as VEGF, PDGF-AA and FGF-b, produced by HUCMSCs, play a role in angiogenesis; thus, HUCMSCs are more angiogenic than BMSCs [34]. In our study, we observed more VEGF-A expression and more CD31+ vessels after HUCMSCs^{Wnt10b} treatment, and that cell culture experiments showed that the HUCMSCs^{Wnt10b} conditioned media could promote tube formation of HUVECs. These findings indicated that the HUCMSCs^{Wnt10b} treatment promoted angiogenesis of endothelial cells, which contributed to accelerated bone defect healing. It remains unknown as to how Wnt10b could regulate VEGF expression, although it can promote endothelial cell proliferation [16], in which VEGF is involved. Furthermore, VEGF is well known for its angiogenic effects on endothelial cells, but we could not exclude the direct effects of VEGF on stem cells, because reduced VEGF resulted in inhibited osteoblast differentiation in MSCs through the regulation of transcription factor RUNX2 [35].

In conclusion, this study is the first one, to our knowledge, that generated HUCMSCs^{Wnt10b}, showed higher self-renewal capacity and showed robust osteogenic differentiation but low adipogenic

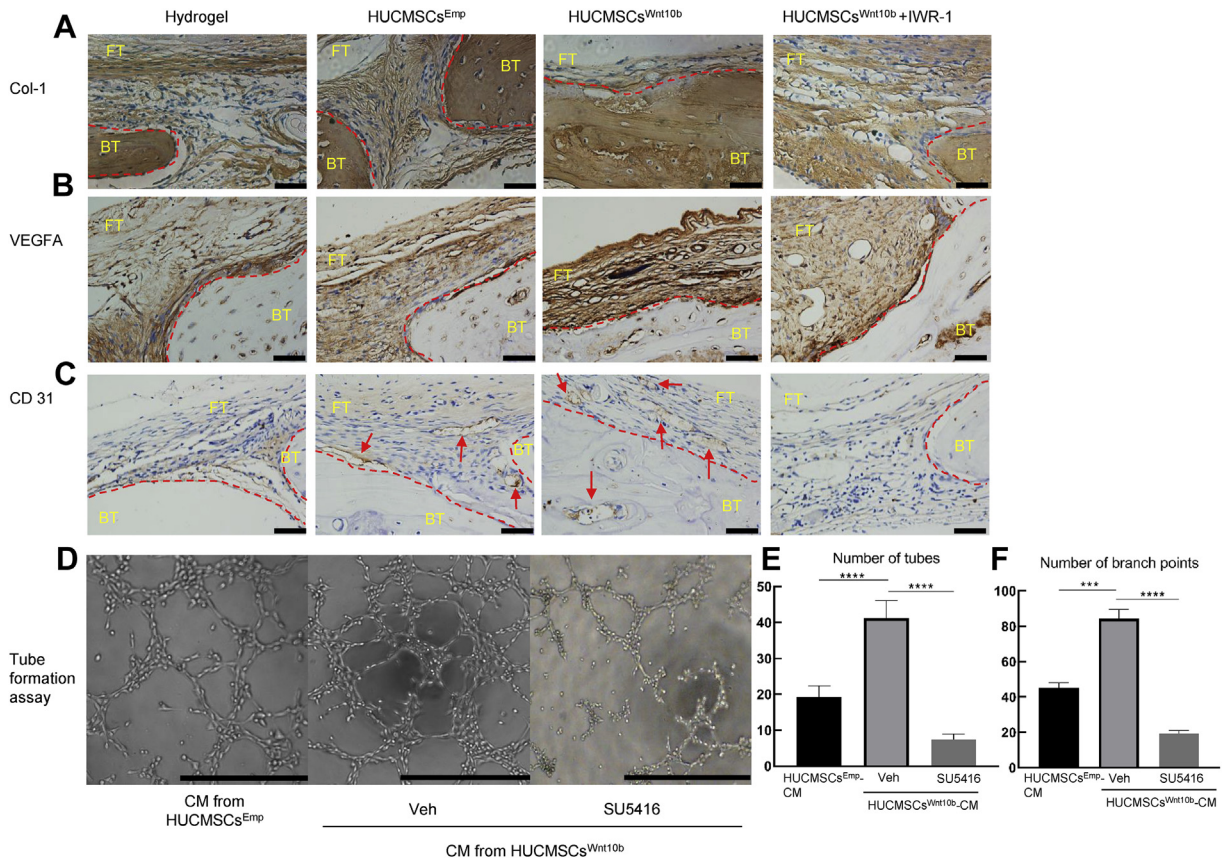

Figure 5. HUCMSCs^{Wnt10b} ameliorated the coupling of angiogenesis and osteogenesis during calvarial defect healing. (A–C) Immunohistochemistry was used to identify VEGF-A (A), CD-31 (B) and collagen-1 (C) expression in calvarial defects at 28 days after operation ($n = 8$, scale bar = 50 μm. FT: fibrous tissue; BT: bone tissue; dashed lines outlined the bone; the red arrows point to CD31+ blood vessels). (D) HUVECs were seeded in 96-well plates at 20,000/well and treated with HUCMSCs^{Emp}-CM, HUCSMCSs^{Wnt10b}-CM and HUCSMCSs^{Wnt10b}-CM + SU5416. 4 h later, pictures were taken under a microscope. Bars = 500 μm. (E, F) The numbers of branch points (E) and tubes (F) were counted ($n = 5$, values represent the mean ± SEM, ***: $p < 0.001$, ****: $p < 0.0001$, Student t test is used for statistics, results are representative of at least three independent experiments).

differentiation ability. We further demonstrated that under *in vivo* settings, HUCMSCs^{Wnt10b} significantly accelerated rat calvarial defect healing and induced more VEGF-A expression and blood vessel growth compared to the control cells. Our study reveals a powerful cell candidate for bone regeneration, which can lay a pathway for clinical translation of stem cell therapy. It sheds lights on future acellular treatment from the powerful cells on bone healing, because cell secretome is gradually considered a main effector of stem cell function. Ultimately, all stakeholders are needed to come together to understand and communicate safety, ethical issues and knowledge about stems cells in order to translate into clinical settings. In the meantime, several questions must be answered before clinical application can take place: (1) What is the interplay between endothelial cells and osteoblastic lineage cells? What is the molecular mechanism of HUCMSCs^{Wnt10b} regulating expression of VEGF? (2) What are the autocrine and paracrine effects of secreted Wnt10b on HUCMSCs^{Wnt10b} and endogenous osteoblastic cells during the healing process? (3) Can HUCMSCs trigger autoimmune response after transplantation? All of these questions warrant further studies in the future.

Conflict of Interest

The authors have no conflicts of interest to disclose in relation to this article.

Acknowledgements

The authors are grateful to Xianrong Zhang from the Department of Orthopaedic Surgery, Nanfang Hospital, Guangzhou, China, for her technical expertise in IHC staining. The authors also thank Roseman University College of Dental Medicine Clinical Outcomes Research and Education in Utah, United States for supporting this study. This study was supported by NSFC grant 81672235 (to Hongtao Tian) and NSFC grant 81702157 (to Wei Tong).

Appendix A. Supplementary data

Supplementary data to this article can be found online at https://doi.org/10.1016/j.jot.2020.02.009.

References

[1] Tzioupis C, Giannoudis PV. Prevalence of long-bone non-unions. Injury 2007; 38(Suppl 2). S3-9.
[2] Blau HM, Daley GQ. Stem cells in the treatment of disease. N Engl J Med 2019; 380(18):1748–60.
[3] Hass R, Kasper C, Bohm S, Jacobs R. Different populations and sources of human mesenchymal stem cells (MSC): a comparison of adult and neonatal tissue-derived MSC. Cell Commun Signal 2011;9:12.
[4] Baksh D, Yao R, Tuan RS. Comparison of proliferative and multilineage differentiation potential of human mesenchymal stem cells derived from umbilical cord and bone marrow. Stem Cell 2007;25(6):1384–92.
[5] Ding DC, Chang YH, Shyu WC, Lin SZ. Human umbilical cord mesenchymal stem cells: a new era for stem cell therapy. Cell Transplant 2015;24(3): 339–47.
[6] Bartolucci J, Verdugo FJ, Gonzalez PL, Larrea RE, Abarzua E, Goset C, et al. Safety and efficacy of the intravenous infusion of umbilical cord mesenchymal stem cells in patients with heart failure: a phase 1/2 randomized controlled trial (RIMECARD trial [randomized clinical trial of intravenous infusion umbilical cord mesenchymal stem cells on cardiopathy]). Circ Res 2017;121(10):1192–204.

[7] Sang WS, Jung IIL, Chi HK, Jong WC, Jee HR, Wonil O, et al. A phase I trial of parenchymal injection of umbilical cord stem cells in Alzheimer's disease. Alzheimer's & Dementia 2013;9(4):P291.
[8] Matas J, Orrego M, Amenabar D, Infante C, Tapia-Limonchi R, Cadiz MI, et al. Umbilical cord-derived mesenchymal stromal cells (MSCs) for knee osteoarthritis: repeated MSC dosing is superior to a single MSC dose and to hyaluronic acid in a controlled randomized phase I/II trial. Stem Cell Transl Med 2019;8(3):215–24.
[9] Zhang Y, Hao Z, Wang P, Xia Y, Wu J, Xia D, et al. Exosomes from human umbilical cord mesenchymal stem cells enhance fracture healing through HIF-1α-mediated promotion of angiogenesis in a rat model of stabilized fracture. Cell Prolif 2019; 52(2):e12570.
[10] Zhou J, Liu HX, Li SH, Gong YS, Zhou MW, Zhang JH, et al. Effects of human umbilical cord mesenchymal stem cells-derived exosomes on fracture healing in rats through the Wnt signaling pathway. Eur Rev Med Pharmacol Sci 2019;23(11): 4954–60.
[11] Todeschi MR, El Backly R, Capelli C, Daga A, Patrone E, Introna M, et al. Transplanted umbilical cord mesenchymal stem cells modify the in vivo microenvironment enhancing angiogenesis and leading to bone regeneration. Stem Cell Dev 2015;24(13):1570–81.
[12] Dilogo IH, Primaputra MRA, Pawitan JA, Liem IK. Modified Masquelet technique using allogeneic umbilical cord-derived mesenchymal stem cells for infected non-union femoral shaft fracture with a 12 cm bone defect: a case report. Int J Surg Case Rep 2017;34:11–6.
[13] Longo KA, Wright WS, Kang S, Gerin L, Chiang SH, Lucas PC, et al. Wnt10b inhibits development of white and brown adipose tissues. J Biol Chem 2004;279(34): 35503–9.
[14] Bennett CN, Longo KA, Wright WS, Suva LJ, Lane TF, Hankenson KD, et al. Regulation of osteoblastogenesis and bone mass by Wnt10b. Proc Natl Acad Sci U S A 2005;102(9):3324–9.
[15] Clevers H, Loh KM, Nusse R. Stem cell signaling. An integral program for tissue renewal and regeneration: Wnt signaling and stem cell control. Science 2014; 346(6205):1248012.
[16] Ishikawa T, Tamai Y, Zorn AM, Yoshida H, Seldin MF, Nishikawa S, et al. Mouse Wnt receptor gene Fzd5 is essential for yolk sac and placental angiogenesis. Development 2001;128(1):25–33.
[17] Zhou D, Qi C, Chen YX, Zhu YJ, Sun TW, Chen F, et al. Comparative study of porous hydroxyapatite/chitosan and whitlockite/chitosan scaffolds for bone regeneration in calvarial defects. Int J Nanomed 2017;12:2673–87.
[18] Spicer PP, Kretlow JD, Young S, Jansen JA, Kasper FK, Mikos AG. Evaluation of bone regeneration using the rat critical size calvarial defect. Nat Protoc 2012;7(10): 1918–29.
[19] Patel ZS, Young S, Tabata Y, Jansen JA, Wong ME, Mikos AG. Dual delivery of an angiogenic and an osteogenic growth factor for bone regeneration in a critical size defect model. Bone 2008;43(5):931–40.
[20] Peng L, Shu X, Lang C, Yu X. Effects of hypoxia on proliferation of human cord blood-derived mesenchymal stem cells. Cytotechnology 2016;68(4):1615–22.
[21] Lee HJ, Ryu JM, Jung YH, Oh SY, Lee SJ, Han HJ. Novel pathway for hypoxia-induced proliferation and migration in human mesenchymal stem cells: involvement of HIF-1α, FASN, and mTORC1. Stem Cell (Dayton, Ohio) 2015;33(7): 2182–95.
[22] Chen W, Liu X, Chen Q, Bao C, Zhao L, Zhu Z, et al. Angiogenic and osteogenic regeneration in rats via calcium phosphate scaffold and endothelial cell co-culture with human bone marrow mesenchymal stem cells (MSCs), human umbilical cord MSCs, human induced pluripotent stem cell-derived MSCs and human embryonic stem cell-derived MSCs. J Tissue Eng Regen Med 2018;12(1):191–203.
[23] Chen W, Baylink DJ, Brier-Jones J, Neises A, Kiroyan JB, Rundle CH, et al. PDGFB-based stem cell gene therapy increases bone strength in the mouse. Proc Natl Acad Sci U S A 2015;112(29):E3893–900.
[24] Bougioukli S, Saitta B, Sugiyama O, Tang AH, Elphingstone J, Evseenko D, et al. Lentiviral gene therapy for bone repair using human umbilical cord blood-derived mesenchymal stem cells. Hum Gene Ther 2019;30(7):906–17.
[25] Li B, Liu W, Zhuang M, Li N, Wu S, Pan S, et al. Overexpression of CD61 promotes hUC-MSC differentiation into male germ-like cells. Cell Prolif 2016;49(1):36–47.
[26] Jerkic M, Masterson C, Ormesher L, Gagnon S, Goyal S, Rabani R, et al. Overexpression of IL-10 enhances the efficacy of human umbilical-cord-derived mesenchymal stromal cells in pneumosepsis. J Clin Med 2019;8(6).
[27] Zhang XS, Linkhart TA, Chen ST, Peng H, Wergedal JE, Guttierez GG, et al. Local ex vivo gene therapy with bone marrow stromal cells expressing human BMP4 promotes endosteal bone formation in mice. J Gene Med 2004;6(1):4–15.
[28] Wilk K, Yeh SA, Mortensen LJ, Ghaffarigarakani S, Lombardo CM, Bassir SH, et al. Postnatal calvarial skeletal stem cells expressing PRX1 reside exclusively in the calvarial sutures and are required for bone regeneration. Stem Cell Rep 2017;8(4): 933–46.
[29] Wang L, Tower RJ, Chandra A, Yao L, Tong W, Xiong Z, et al. Periosteal mesenchymal progenitor dysfunction and extraskeletally-derived fibrosis contribute to atrophic fracture nonunion. J Bone Miner Res 2019;34(3):520–32.
[30] Paik DT, Rai M, Ryzhov S, Sanders LN, Aisagbonhi O, Funke MJ, et al. Wnt10b gain-of-function improves cardiac repair by arteriole formation and attenuation of fibrosis. Circ Res 2015;117(9):804–16.
[31] Hu K, Olsen BR. Osteoblast-derived VEGF regulates osteoblast differentiation and bone formation during bone repair. J Clin Invest 2016;126(2):509–26.
[32] Day TF, Guo X, Garrett-Beal L, Yang Y. Wnt/beta-catenin signaling in mesenchymal progenitors controls osteoblast and chondrocyte differentiation during vertebrate skeletogenesis. Dev Cell 2005;8(5):739–50.
[33] Liu F, Kohlmeier S, Wang CY. Wnt signaling and skeletal development. Cell Signal 2008;20(6):999–1009.
[34] Balasubramanian S, Venugopal P, Sundarraj S, Zakaria Z, Majumdar AS, Ta M. Comparison of chemokine and receptor gene expression between Wharton's jelly and bone marrow-derived mesenchymal stromal cells. Cytotherapy 2012;14(1):26–33.
[35] Liu Y, Berendsen AD, Jia S, Lotinun S, Baron R, Ferrara N, et al. Intracellular VEGF regulates the balance between osteoblast and adipocyte differentiation. J Clin Invest 2012;122(9):3101–13.